Available online at www.sciencedirect.com
SCIENCE DIRECT®
Journal of Computational Physics 212 (2006) 718–738
JOURNAL OF COMPUTATIONAL PHYSICS
www.elsevier.com/locate/jcp

Far-field approximation for hydrodynamic interactions in parallel-wall geometry

S. Bhattacharya, J. Bławzdziewicz *, E. Wajnryb [1]

Department of Mechanical Engineering, Yale University, Manson Laboratory, Room M2, P.O. Box 208286, New Haven, CT 06520-8286, USA

Received 26 April 2005; received in revised form 22 July 2005; accepted 25 July 2005
Available online 6 September 2005

Abstract

A complete analysis is presented for the far-field creeping flow produced by a multipolar force distribution in a fluid confined between two parallel planar walls. We show that at distances larger than several wall separations the flow field assumes the Hele–Shaw form, i.e. it is parallel to the walls and varies quadratically in the transverse direction. The associated pressure field is a two-dimensional harmonic function that is characterized by the same multipolar number m as the original force multipole. Using these results we derive asymptotic expressions for the Green's matrix that represents Stokes flow in the wall-bounded fluid in terms of a multipolar spherical basis. This Green's matrix plays a central role in our recently proposed algorithm [Physica A 356 (2005) 294] for evaluating many-body hydrodynamic interactions in a suspension of spherical particles in the parallel-wall geometry. Implementation of our asymptotic expressions in this algorithm increases its efficiency substantially because the numerically expensive evaluation of the exact matrix elements is needed only for the neighboring particles. Our asymptotic analysis will also be useful in developing hydrodynamic algorithms for wall-bounded periodic systems and implementing acceleration methods by using corresponding results for the two-dimensional scalar potential.

Keywords: Hydrodynamic interactions; Confined systems; Stokes flow; Suspensions; Hele–Shaw flow

1. Introduction

Numerical and theoretical investigations of particle motion in suspensions bounded by planar walls require efficient methods for evaluating hydrodynamic interactions in these systems. Examples of phenomena

* Corresponding author. Tel.: +1 203 432 7754; fax: +1 203 432 7654.
E-mail address: jerzy.blawzdziewicz@yale.edu (J. Bławzdziewicz).
[1] On leave from IPPT Warsaw, Poland.

0021-9991/$ - see front matter © 2005 Elsevier Inc. All rights reserved.
doi:10.1016/j.jcp.2005.07.015

where the hydrodynamic wall effects are important include collective particle motion in quasi-bidimensional colloidal suspensions [1–5], and conformation dynamics of a DNA molecule in a parallel-plate microchannel [6].

Several methods for evaluating hydrodynamic interactions in wall-bounded systems have been proposed. In some studies, the flow reflected from the walls was calculated numerically using either boundary-integral [7] or finite-difference [6] techniques. In a different approach [8], the exact point-force solution for the flow between the walls [9] was used. Wall effects were also included using a multiple-reflection technique [10], and several approximation methods were proposed [11–13]. While all of these methods have their merits, they also have some essential disadvantages, such as a high numerical cost or an insufficient (in many cases unknown) accuracy.

Recently we have derived [14,15], a novel algorithm for evaluating hydrodynamic friction matrix in a wall-bounded suspension of spheres under creeping-flow conditions.[2] Our Cartesian-representation method relies on transformations between a spherical basis set of solutions of Stokes equations (this set is consistent with the particle geometry) and a Cartesian basis set (which is consistent with the wall geometry). The algorithm provides highly accurate results for multiparticle friction and mobility matrices.

Using our approach, we have obtained several interesting numerical results. In particular, we have shown that the friction matrix undergoes a crossover from the quasi-three-dimensional to quasi-two-dimensional form when the interparticle distance becomes larger than the wall separation H. We have also observed an unusually large resistance coefficient for a long rigid chain of spheres in transverse motion (with respect to the orientation of the chain) in a narrow, wall-bounded space. Since both these effects involve flow on the length scale $l \gg H$, they are not captured by the usual single-wall superposition approximation which does not properly take the far-field flow into account (as demonstrated in [14]).

Large-scale studies of particle dynamics in the two-wall geometry require efficient simulation algorithms. In our approach [14,15] the most expensive part is evaluation of the Green's matrix G in the multipolar representation. This matrix is a key quantity in our algorithm—its elements correspond to the coefficients in the expansion of the hydrodynamic Green's tensor for the wall-bounded system into multipolar basis fields. The inverse of the Green's matrix combined with the one-particle reflection matrices yields the multiparticle hydrodynamic friction matrix.

In our algorithm [14,15] the matrix G is expressed in terms of lateral Fourier integrals with respect to the two-dimensional wave vector in a plane parallel to the walls. Evaluation of these integrals is especially difficult for widely separated particles due to the oscillatory character of the integrands. In the present paper we derive much simpler asymptotic formulas for the matrix G in the far-field regime. When the particle separation is sufficiently large, these formulas can be used instead of the Fourier integrals, resulting in a significant reduction of numerical cost (and in other important simplifications).

Our analysis of the asymptotic form of the matrix G relies on the observation that in the far-field regime the velocity field in the space between the walls assumes a simple Hele–Shaw (i.e. the lubrication) form. Accordingly, the flow field has only the lateral components and it varies quadratically across the space between the walls. Such a flow field is entirely determined by the corresponding pressure field, which is a two-dimensional harmonic function that depends only on the lateral coordinates. It follows that at large distances $r \gg H$, the full three-dimensional hydrodynamic problem is reduced to a much simpler two-dimensional scalar problem for the pressure.

This paper is organized as follows. Our method [14,15] for evaluating many-particle hydrodynamic interactions in the parallel-wall geometry is summarized in Sections 2 and 3. Section 2 recalls the induced-force formulation of the problem, and Section 3 summarizes the force-multipole expansion method. The main theoretical results of the present analysis are given in Section 4, where the Hele–Shaw approximation for the far-field flow is discussed, and explicit expressions for Green's matrix G are derived. In Section 5, we

[2] An algorithm based on similar ideas was also developed by Jones [16].

present some results of numerical calculations. We show the dependence of Green's matrix elements on the interparticle distance, and we illustrate the role of their far-field behavior in the description of hydrodynamic interactions in rigid arrays of spheres. Concluding remarks are given in Section 6, and some technical details are presented in the appendices.

2. Multiparticle hydrodynamic interactions

2.1. Hydrodynamic resistance

We consider the motion of N spherical particles of the radius a, which are suspended in a fluid of viscosity η, under creeping-flow conditions. The system is bounded by two planar parallel walls at the positions $z = 0$ and $z = H$, where $\mathbf{r} = (x, y, z)$ are the Cartesian coordinates. The centers of particles $i = 1, \ldots, N$ are at positions $\mathbf{R}_i = (X_i, Y_i, Z_i)$, and the translational and rotational particle velocities are $\mathbf{U}_i$ and $\mathbf{\Omega}_i$. The external forces and torques acting on the particles are denoted by $\mathscr{F}_i$ and $\mathscr{T}_i$. It is assumed that the flow field satisfies the no-slip boundary conditions on the particle surfaces and the walls.

For a system of spheres undergoing translational and rotational rigid-body motion with no external flow, the particle dynamics is characterized by the resistance matrix

$$\zeta_{ij} = \begin{bmatrix} \zeta_{ij}^{\mathrm{tt}} & \zeta_{ij}^{\mathrm{tr}} \\ \zeta_{ij}^{\mathrm{rt}} & \zeta_{ij}^{\mathrm{rr}} \end{bmatrix}, \quad i, j = 1, \ldots, N, \tag{1}$$

defined by the linear relation

$$\begin{bmatrix} \mathscr{F}_i \\ \mathscr{T}_i \end{bmatrix} = \sum_{j=1}^{N} \begin{bmatrix} \zeta_{ij}^{\mathrm{tt}} & \zeta_{ij}^{\mathrm{tr}} \\ \zeta_{ij}^{\mathrm{rt}} & \zeta_{ij}^{\mathrm{rr}} \end{bmatrix} \cdot \begin{bmatrix} \mathbf{U}_j \\ \mathbf{\Omega}_j \end{bmatrix}. \tag{2}$$

The dot in the above equation denotes the matrix multiplication and contraction of the Cartesian tensorial components of the resistance matrix. Our goal is to calculate the resistance matrix $\boldsymbol{\zeta}$, or its inverse, the mobility matrix $\boldsymbol{\mu}$. Our method [14,15] for evaluating these quantities is outlined below.

2.2. Induced-force formulation

The effect of the suspended particles on the surrounding fluid can be described in terms of the induced-force distributions on the particle surfaces. These distributions can be written in a form

$$\mathbf{F}_i(\mathbf{r}) = \delta_a^{\mathrm{S}}(\mathbf{r} - \mathbf{R}_i)\mathbf{f}_i(\mathbf{r}), \tag{3}$$

where

$$\delta_a^{\mathrm{S}}(\mathbf{r}) = a^{-2}\delta(r - a). \tag{4}$$

By the definition of the induced force [17–19], the flow field

$$\mathbf{v}(\mathbf{r}) = \sum_{i=1}^{N} \int \mathbf{T}(\mathbf{r}, \mathbf{r}') \cdot \mathbf{F}_i(\mathbf{r}')\mathrm{d}\mathbf{r}' \tag{5}$$

is identical to the velocity field in the presence of the moving particles. Here

$$\mathbf{T}(\mathbf{r}, \mathbf{r}') = \mathbf{T}_0(\mathbf{r} - \mathbf{r}') + \mathbf{T}'(\mathbf{r}, \mathbf{r}') \tag{6}$$

is the Green's function for the Stokes flow in the presence of the boundaries; the Green's function $\mathbf{T}(\mathbf{r}, \mathbf{r}')$ is decomposed into the Oseen tensor

$$\mathbf{T}_0(\mathbf{r}) = \frac{1}{8\pi\eta r}(\hat{\mathbf{I}} + \hat{\mathbf{r}}\hat{\mathbf{r}}) \tag{7}$$

and the part $\mathbf{T}'(\mathbf{r},\mathbf{r}')$ that describes the flow reflected from the walls. In Eq. (5), it is assumed that the particles move with given velocities, but no external flow is imposed.

The resistance relation (2) is linked to the induced-force distributions (3) through the expressions

$$\mathscr{F}_i = \int \mathbf{F}_i(\mathbf{r})\mathrm{d}\mathbf{r}, \quad \mathscr{T}_i = \int \mathbf{r}_i \times \mathbf{F}_i(\mathbf{r})\mathrm{d}\mathbf{r} \tag{8}$$

for the total force and torque, respectively. To determine the resistance matrix (1) we thus need to evaluate the induced forces (3) for given translational and angular velocities of the particles.

2.3. Boundary-integral equations for the induced forces

For a system of particles moving with the translational and angular velocities $\mathbf{U}_i$ and $\mathbf{\Omega}_i$, the induced-force distribution (3) can be obtained from the boundary-integral equation

$$[\mathbf{Z}_i^{-1}\mathbf{F}_i](\mathbf{r}) + \sum_{j=1}^{N} \int [\delta_{ij}\mathbf{T}'(\mathbf{r}-\mathbf{r}') + (1-\delta_{ij})\mathbf{T}(\mathbf{r}-\mathbf{r}')] \cdot \mathbf{F}_j(\mathbf{r}')\mathrm{d}\mathbf{r}' = \mathbf{v}_i^{\mathrm{rb}}(\mathbf{r}), \quad \mathbf{r} \in S_i, \tag{9}$$

where

$$\mathbf{v}_i^{\mathrm{rb}}(\mathbf{r}) = \mathbf{U}_i + \mathbf{\Omega}_i \times \mathbf{r}_i \tag{10}$$

is the rigid-body velocity field associated with the particle motion, and S_i is the surface of particle i. In the boundary-integral equation (9), $\mathbf{Z}_i$ denotes the one-particle scattering operator that describes the response of an individual particle to an external flow in an unbounded space. This operator is defined by the linear relation

$$\mathbf{F}_i = -\mathbf{Z}_i(\mathbf{v}_i^{\mathrm{in}} - \mathbf{v}_i^{\mathrm{rb}}), \tag{11}$$

where $\mathbf{v}_i^{\mathrm{in}}$ is the velocity incident to particle i. For specific particle models (e.g., rigid particles or drops), explicit expressions for the operator $\mathbf{Z}_i$ are known [20–22].

3. Force-multipole expansion

3.1. Spherical basis fields

As in a standard force-multipole approach [23,24] the boundary-integral equation (9) is transformed into a linear matrix equation by projecting it onto a spherical basis of Stokes flow. To this end we use the reciprocal basis sets defined by Cichocki et al. [21]. We introduce, however, a slightly different normalization to exploit the full symmetry of the problem.

The singular and nonsingular spherical basis solutions of Stokes equations $\mathbf{v}^-_{lm\sigma}(\mathbf{r})$ and $\mathbf{v}^+_{lm\sigma}(\mathbf{r})$ (with $l = 1,2,\ldots$, $m = -l,\ldots,l$ and $\sigma = 0,1,2$) have the following separable form in the spherical coordinates $\mathbf{r} = (r,\theta,\phi)$:

$$\mathbf{v}^-_{lm\sigma}(\mathbf{r}) = \mathbf{V}^-_{lm\sigma}(\theta,\phi)r^{-(l+\sigma)}, \tag{12a}$$

$$\mathbf{v}^+_{lm\sigma}(\mathbf{r}) = \mathbf{V}^+_{lm\sigma}(\theta,\phi)r^{l+\sigma-1}. \tag{12b}$$

The coefficients $\mathbf{V}^{-}_{lm\sigma}(\theta,\phi)$ and $\mathbf{V}^{+}_{lm\sigma}(\theta,\phi)$ are combinations of vector spherical harmonics with angular order l and azimuthal order m. This property and the r-dependence in Eq. (12) define the Stokes-flow fields $\mathbf{v}^{\pm}_{lm\sigma}(\mathbf{r})$ up to normalization.

We use here a convenient normalization introduced in [15], which emphasizes various symmetries of the problem. Explicit expressions for the functions $\mathbf{V}^{\pm}_{lm\sigma}$ in this normalization are given in Appendix A. We note that both in our present and in the original normalization [21], the basis fields $\mathbf{v}^{-}_{lm\sigma}$ satisfy the identity [25]

$$\eta\mathbf{T}_0(\mathbf{r}-\mathbf{r}') = \begin{cases} \sum_{lm\sigma} \mathbf{v}^{-}_{lm\sigma}(\mathbf{r})\mathbf{v}^{+*}_{lm\sigma}(\mathbf{r}'), & r > r', \quad \text{(a)} \\ \sum_{lm\sigma} \mathbf{v}^{+}_{lm\sigma}(\mathbf{r})\mathbf{v}^{-*}_{lm\sigma}(\mathbf{r}'), & r < r', \quad \text{(b)} \end{cases} \tag{13}$$

where $\mathbf{T}_0(\mathbf{r}-\mathbf{r}')$ is the Oseen tensor (7). Relation (13) assures that the Lorentz reciprocal symmetry of Stokes flow is reflected in the symmetry of the resulting matrix representation of the problem [24].

Following [21] we also introduce the reciprocal basis fields $\mathbf{w}^{\pm}_{lm\sigma}(\mathbf{r})$, defined by the orthogonality relations of the form

$$\langle \delta^{\mathrm{S}}_a \mathbf{w}^{\pm}_{lm\sigma} | \mathbf{v}^{\pm}_{l'm'\sigma'} \rangle = \delta_{ll'}\delta_{mm'}\delta_{\sigma\sigma'}. \tag{14}$$

Here

$$\langle \mathbf{A}|\mathbf{B}\rangle = \int \mathbf{A}^*(\mathbf{r})\cdot\mathbf{B}(\mathbf{r})\mathrm{d}\mathbf{r} \tag{15}$$

is the inner product, the asterisk denotes the complex conjugate, and $\delta^{\mathrm{S}}_{\mathrm{a}}$ is defined in Eq. (4). The reciprocal basis fields and the bra–ket notation (15) allows us to conveniently represent expansions of Stokes flow fields into the complete sets of nonsingular and singular basis fields (12). In particular, any Stokes flow $\mathbf{u}(\mathbf{r})$ that is nonsingular in the neighborhood of a point $\mathbf{r} = \mathbf{R}_i$ has an expansion

$$\mathbf{u}(\mathbf{r}) = \sum_{lm\sigma} \mathbf{v}^{+}_{lm\sigma}(\mathbf{r}-\mathbf{R}_i)\langle \delta^{\mathrm{S}}_a(i)\mathbf{w}^{+}_{lm\sigma}(i)|\mathbf{u}\rangle, \tag{16}$$

where

$$\mathbf{w}^{+}_{lm\sigma}(i) \equiv \mathbf{w}^{+}_{lm\sigma}(\mathbf{r}-\mathbf{R}_i), \tag{17a}$$

$$\delta^{\mathrm{S}}_a(i) \equiv \delta^{\mathrm{S}}_a(\mathbf{r}-\mathbf{R}_i). \tag{17b}$$

3.2. Matrix representation

The matrix representation of the boundary-integral equation (9) is obtained using the multipolar expansion

$$\mathbf{F}_i(\mathbf{r}) = \sum_{lm\sigma} f_i(lm\sigma)\delta^{\mathrm{S}}_a(\mathbf{r}-\mathbf{R}_i)\mathbf{w}^{+}_{lm\sigma}(\mathbf{r}-\mathbf{R}_i) \tag{18}$$

of the induced-force distributions (3). The multipolar moments in the above expression are given by the projection

$$f_i(lm\sigma) = \langle \mathbf{v}^{+}_{lm\sigma}(i)|\mathbf{F}_i\rangle, \tag{19}$$

according to the orthogonality condition (14). The definition (19) of the multipolar expansion is justified by the identity

$$\mathbf{v}^{-}_{lm\sigma}(\mathbf{r}) = \eta\int \mathbf{T}_0(\mathbf{r}-\mathbf{r}')\delta^{\mathrm{S}}_a(\mathbf{r}')\mathbf{w}^{+}_{lm\sigma}(\mathbf{r}')\mathrm{d}\mathbf{r}', \tag{20}$$

which follows from the representation (13) of the Oseen tensor. Eqs. (18) and (20) indicate that the multipolar moments $f_i(lm\sigma)$ are identical (apart from the trivial factor η) to the expansion coefficients of the flow field scattered by an isolated particle in unbounded space into the singular basis fields $\mathbf{v}^-_{lm\sigma}$.

To obtain a linear matrix equation for the set of force multipolar moments $f_i(lm\sigma)$, representation (18) is inserted into the boundary-integral equation (9), and the resulting expression is expanded into the nonsingular basis fields (12b), which yields

$$\sum_{j=1}^{N}\sum_{l'm'\sigma'} M_{ij}(lm\sigma|l'm'\sigma')f_j(l'm'\sigma') = c_i(lm\sigma). \tag{21}$$

For a particle moving in a quiescent fluid, the coefficients

$$c_i(lm\sigma) = \langle \delta^{\mathrm{S}}_a(i)\mathbf{w}^+_{lm\sigma}(i)|\mathbf{v}^{\mathrm{rb}}_i\rangle \tag{22}$$

on the right-hand side are nonzero only for $l = 1$ and $\sigma = 0, 1$. The matrix M in Eq. (21) consists of three contributions corresponding to the three terms on the left side of Eq. (9),

$$M_{ij}(lm\sigma|l'm'\sigma') = \delta_{ij}\delta_{ll'}\delta_{mm'}Z^{-1}_i(l;\sigma|\sigma') + \delta_{ij}G'_{ij}(lm\sigma|l'm'\sigma') + (1-\delta_{ij})G_{ij}(lm\sigma|l'm'\sigma'). \tag{23}$$

Using the bra–ket notation these contributions can be expressed in the form

$$Z^{-1}_i(l;\sigma|\sigma') = \langle \delta^{\mathrm{S}}_a(i)\mathbf{w}^+_{lm\sigma}(i)|\mathbf{Z}^{-1}_i|\delta^{\mathrm{S}}_a(i)\mathbf{w}^+_{lm\sigma'}(i)\rangle, \tag{24}$$

$$G'_{ii}(lm\sigma|l'm'\sigma') = \langle \delta^{\mathrm{S}}_a(i)\mathbf{w}^+_{lm\sigma}(i)|\mathbf{T}'|\delta^{\mathrm{S}}_a(i)\mathbf{w}^+_{l'm'\sigma'}(i)\rangle \tag{25}$$

and

$$G_{ij}(lm\sigma|l'm'\sigma') = \langle \delta^{\mathrm{S}}_a(i)\mathbf{w}^+_{lm\sigma}(i)|\mathbf{T}|\delta^{\mathrm{S}}_a(j)\mathbf{w}^+_{l'm'\sigma'}(j)\rangle. \tag{26}$$

The first term $Z^{-1}_i(l;\sigma|\sigma')$ is associated with the one particle operator $\mathbf{Z}^{-1}_i$ in Eq. (9), and it relates the force multipoles $f_i(l'm'\sigma')$ induced on particle i to the coefficients in the expansion of the flow field incoming to this particle into the nonsingular spherical basis fields (12b). By the spherical symmetry, this term is diagonal in the indices l and m and is independent of m. The Green's matrices $G'_{ij}(lm\sigma|l'm'\sigma')$ and $G_{ij}(lm\sigma|l'm'\sigma')$ are associated with the integral operators that involve the kernels $\mathbf{T}'(\mathbf{r},\mathbf{r}')$ and $\mathbf{T}(\mathbf{r},\mathbf{r}')$. Using the orthogonality relations (14) one can show that the elements of these matrices correspond to the expansion of the flow produced by a force multipole centered at $\mathbf{R}_j$ into the nonsingular basis (12b) centered at $\mathbf{R}_i$.

Explicit expressions for the single-particle reflection matrix Z^{-1}_i are well known [21,26]. Quadrature formulas for the Green's matrix G_{ij}have been derived in our recent publication [15], where the matrix elements $G_{ij}(lm\sigma|l'm'\sigma')$ are represented as a combination of the free-space Green's matrix [26,24] and the wall contribution $G'_{ij}(lm\sigma|l'm'\sigma')$ that is given in a form of a Hankel transform of a product of several simple matrices. The Hankel transform arises from angular integration of lateral Fourier modes of Stokes flow.

The many-particle resistance matrix (1) can be obtained by solving Eq. (21) and projecting the induced force multipoles onto the total force and torque (8). Explicit expressions for the resistance matrix in terms of the generalized friction matrix M^{-1} are given in [15]. In numerical applications, the system of linear equation (21) is truncated at a given multipolar order l, and the resulting approximate friction matrix is supplemented with a lubrication correction (as described in [15]).

4. Far-field approximation

Calculation of the exact matrix elements $G_{ij}(lm\sigma|l'm'\sigma')$ by our Cartesian-representation method [15] requires numerical evaluation of Hankel transforms that involve the Bessel functions $J_{m-m'}(k\varrho_{ij})$. Here k is the magnitude of the lateral wave vector, and $\varrho_{ij} = |\boldsymbol{\varrho}_i - \boldsymbol{\varrho}_j|$, where $\boldsymbol{\varrho}_i = (X_i, Y_i)$ denotes the lateral position of

particle i. For large interparticle distances ϱ_{ij}, the factor $J_{m-m'}(k\varrho_{ij})$ undergoes rapid oscillations as a function of k. Thus, evaluation of the Fourier integrals in the Hankel transforms is numerically expensive for such configurations.

In the following sections, we derive explicit asymptotic expressions for the matrix elements $G_{ij}(lm\sigma|l'm'\sigma')$ at large interparticle distances $\varrho_{ij} \gg H$. As we will see, these expressions have a very simple form, and do not require evaluation of the Fourier integrals.

4.1. Hele–Shaw form of the far-field flow

Our asymptotic analysis relies on the observation that in the far-field regime the flow between two parallel walls assumes the Hele–Shaw form. Accordingly, the asymptotic pressure field $p = p^{\mathrm{as}}$ varies only in the lateral direction, and the associated flow field has the lubrication form

$$\mathbf{u}^{\mathrm{as}}(\mathbf{r}) = -\frac{1}{2}\eta^{-1} z(H-z)\nabla_{\parallel} p^{\mathrm{as}}(\boldsymbol{\rho}), \tag{27}$$

where

$$\mathbf{r} = \boldsymbol{\rho} + z\hat{\mathbf{e}}_z \tag{28}$$

and $\nabla_{\parallel}$ is the two-dimensional gradient operator with respect to the lateral position $\boldsymbol{\rho} = (x, y)$. By the incompressibility of the flow field (27), the pressure field p^{as} satisfies the two-dimensional Laplace's equation

$$\nabla_{\parallel}^2 p^{\mathrm{as}}(\boldsymbol{\rho}) = 0. \tag{29}$$

The asymptotic expressions (27) and (29) can be obtained [27] by expanding the boundary-value problem for Stokes flow in the space between the walls in the small parameter $H/\rho \ll 1$, where ρ is the distance from the force distribution that generates the fluid motion. Since the velocity field (27) itself satisfies the Stokes equations and boundary conditions exactly, one can show that the higher-order terms in the asymptotic expansion vanish. This property indicates that the correction terms are subdominant [28], which in turn suggests that the asymptotic behavior (27) and (29) is approached exponentially. This conclusion is consistent with the direct analysis of the asymptotic form of the Green's function in the space between the walls by Liron and Mochon [9] (see the discussion in Section 4.4 below).

4.2. Asymptotic basis sets

To find the far-field form of the velocity field produced by induced-force multipoles and to obtain the corresponding asymptotic expressions for the elements of the Green's matrix $G_{ij}(lm\sigma|l'm'\sigma')$, it is convenient to define appropriate basis sets of Hele–Shaw flow and pressure fields. The sets of singular and nonsingular pressures are defined by the relation

$$q_m^{\mathrm{as}\pm}(\boldsymbol{\rho}) = \eta \Phi_m^{\pm}(\boldsymbol{\rho}), \tag{30}$$

where $m = 0, \pm 1, \pm 2, \ldots$, and

$$\Phi_0^{-}(\boldsymbol{\rho}) = -\ln\rho, \quad \Phi_m^{-}(\boldsymbol{\rho}) = \frac{1}{2|m|}\rho^{-|m|}\mathrm{e}^{\mathrm{i}m\phi}, \quad m \neq 0, \tag{31a}$$

$$\Phi_m^{+}(\boldsymbol{\rho}) = \rho^{|m|}\mathrm{e}^{\mathrm{i}m\phi} \tag{31b}$$

are the two-dimensional harmonic basis functions. The associated Hele–Shaw basis velocity fields are

$$\mathbf{v}_m^{\mathrm{as}\pm}(\mathbf{r}) = -\frac{1}{2} z(H-z)\nabla_{\parallel}\Phi_m^{\pm}(\boldsymbol{\rho}), \tag{32}$$

according to Eq. (27).

Below we list several useful relations for the harmonic functions (31). First, we have the diagonal representation for the Green's function

$$\Phi_0^-(\boldsymbol{\rho}-\boldsymbol{\rho}') = \begin{cases} \sum_{m=-\infty}^{\infty} \Phi_m^-(\boldsymbol{\rho})\Phi_m^{+*}(\boldsymbol{\rho}'), & \rho > \rho', \quad \text{(a)} \\ \sum_{m=-\infty}^{\infty} \Phi_m^+(\boldsymbol{\rho})\Phi_m^{-*}(\boldsymbol{\rho}'), & \rho < \rho', \quad \text{(b)} \end{cases} \tag{33}$$

which is analogous to the representation (13) of the Oseen tensor. Next, we also have the displacement theorem

$$\Phi_{m'}^-(\boldsymbol{\rho}-\boldsymbol{\varrho}_j) = \sum_{m=-\infty}^{\infty} \Phi_m^+(\boldsymbol{\rho}-\boldsymbol{\varrho}_i) S_{\mathrm{cyl}}^{+-}(\boldsymbol{\varrho}_{ij}; m|m'), \tag{34}$$

where $\boldsymbol{\varrho}_{ij} = \boldsymbol{\varrho}_i - \boldsymbol{\varrho}_j$, and the displacement matrix is given by

$$S_{\mathrm{cyl}}^{+-}(\boldsymbol{\varrho}; m|m') = \theta(-mm')(-1)^{m'} \frac{(|m|+|m'|)!}{|m|!|m'|!} \Phi_{m'-m}^-(\boldsymbol{\varrho}). \tag{35}$$

We note that due to the presence of the Heaviside step function

$$\theta(x) = \begin{cases} 0, & x < 0, \\ 1, & x \geqslant 0 \end{cases} \tag{36}$$

in Eq. (35), the scalar fields with the same sign of the indices $m, m' \neq 0$ do not couple in the displacement relation (34). We also note that the matrix (35) satisfies the symmetry relation

$$S_{\mathrm{cyl}}^{+-}(\boldsymbol{\varrho}; m|m') = S_{\mathrm{cyl}}^{+-*}(-\boldsymbol{\varrho}; m'|m). \tag{37}$$

As a direct consequence of the displacement theorem (34) for the scalar pressure fields, we have the corresponding displacement relation for the Hele–Shaw basis flows (32)

$$\mathbf{v}_{m'}^{\mathrm{as}-}(\mathbf{r}-\boldsymbol{\varrho}_j) = \sum_{m=-\infty}^{\infty}{}' \mathbf{v}_m^{\mathrm{as}+}(\mathbf{r}-\boldsymbol{\varrho}_i) S_{\mathrm{cyl}}^{+-}(\boldsymbol{\varrho}_{ij}; m|m'). \tag{38}$$

The term with $m = 0$ in the above relation vanishes because $\mathbf{v}_0^{\mathrm{as}+} \equiv 0$ according to Eqs. (31b) and (32). The prime at the summation sign has been introduced to emphasize that this term is omitted.

In the following section, we will derive a diagonal representation (analogous to (13) and (33)) for the hydrodynamic Green's tensor describing the asymptotic far-field response of the fluid confined between walls to a point force.

4.3. Asymptotic Green's tensor

An explicit expression for the far-field flow produced by a point force in the space between the walls has been derived by Liron and Mochon [9] (see also [29]). According to their results, the far-field flow produced by a force $\mathbf{F}$ applied at the position $(0,0,z')$ can be expressed in the form

$$\mathbf{u}(\mathbf{r}) = \frac{3}{2}\pi^{-1}\eta^{-1}H^{-3}z(H-z)z'(H-z')\boldsymbol{\nabla}_{\parallel}\boldsymbol{\nabla}_{\parallel}(-\ln\rho)\cdot\mathbf{F} + o(\mathrm{e}^{-\rho/H}). \tag{39}$$

The above relation can also be obtained by a direct expansion of the boundary-value problem in the small parameter H/ρ [27].

Relation (39) indicates that the correction to the far-field $O(\rho^{-2})$ asymptotic behavior of the fluid velocity $\mathbf{u}$ decays exponentially with ρ. Moreover, the vertical component of the force $\mathbf{F}$ does not contribute to the $O(\rho^{-2})$ behavior.

Eq. (39) can be rephrased as an expression for the asymptotic form $\mathbf{T}^{\mathrm{as}}$ of the full Green's function (6)

$$\mathbf{T}^{\mathrm{as}}(\mathbf{r},\mathbf{r}') = -\frac{3}{2}\pi^{-1}\eta^{-1}H^{-3}z(H-z)z'(H-z')\nabla_{\parallel}\nabla'_{\parallel}(-\ln|\boldsymbol{\rho}-\boldsymbol{\rho}'|), \tag{40}$$

where $\mathbf{r}' = \boldsymbol{\rho}' + z'\hat{\mathbf{e}}_z$. One of the gradient operators in the above formula has been applied to the primed coordinates to emphasize the Lorentz symmetry of the Green's tensor

$$\mathbf{T}^{\mathrm{as}}(\mathbf{r},\mathbf{r}') = \mathbf{T}^{\mathrm{as}\dagger}(\mathbf{r}',\mathbf{r}) \tag{41}$$

(where the dagger denotes the transpose of the tensor). Due to the translational invariance of the system in the lateral directions, the Green's function (40) satisfies the identity

$$\mathbf{T}^{\mathrm{as}}(\mathbf{r}-\boldsymbol{\varrho},\mathbf{r}'-\boldsymbol{\varrho}) = \mathbf{T}^{\mathrm{as}}(\mathbf{r},\mathbf{r}'), \tag{42}$$

where the vector $\boldsymbol{\varrho}$ has only lateral components.

Using Eqs. (32) and (33) and noting that the Green's function (40) is quadratic both in primed and unprimed transverse variables, we find the relation

$$\mathbf{T}^{\mathrm{as}}(\mathbf{r},\mathbf{r}') = -\frac{6}{\pi\eta H^3}\begin{cases} {\sum_{m=-\infty}^{\infty}}' \mathbf{v}_m^{\mathrm{as}-}(\mathbf{r})\mathbf{v}_m^{\mathrm{as}+*}(\mathbf{r}'), & \rho > \rho', \quad \text{(a)} \\ {\sum_{m=-\infty}^{\infty}}' \mathbf{v}_m^{\mathrm{as}+}(\mathbf{r})\mathbf{v}_m^{\mathrm{as}-*}(\mathbf{r}'), & \rho < \rho', \quad \text{(b)} \end{cases} \tag{43}$$

which is analogous to the diagonal representation of the Oseen tensor (13). Eq. (43a) combined with the displacement theorem for the Hele–Shaw basis fields (38) and identity (42) yields the symmetric representation of the asymptotic Green's tensor (40)

$$\mathbf{T}^{\mathrm{as}}(\mathbf{r},\mathbf{r}') = -\frac{6}{\pi\eta H^3}{\sum_{m=-\infty}^{\infty}}'{\sum_{m'=-\infty}^{\infty}}' \mathbf{v}_m^{\mathrm{as}+}(\mathbf{r}-\boldsymbol{\varrho}_i)S_{\mathrm{cyl}}^{+-}(\boldsymbol{\varrho}_{ij};m|m')\mathbf{v}_{m'}^{\mathrm{as}+*}(\mathbf{r}'-\boldsymbol{\varrho}_j). \tag{44}$$

4.4. Asymptotic form of the two-wall Green's matrix

The asymptotic form of the matrix elements (26) can be obtained by projecting relation (44) onto the reciprocal basis fields $\mathbf{w}^{+}_{lm\sigma}$ centered at the points $\mathbf{R}_i$ and $\mathbf{R}_j$. The resulting expression involves the matrix elements

$$\langle \delta_a^{\mathrm{S}}(i)\mathbf{w}^{+}_{lm\sigma}(i)|\mathbf{v}^{\mathrm{as}+}_{m'}(i)\rangle = \delta_{mm'}C(Z_i;lm\sigma), \tag{45}$$

where $\mathbf{v}^{\mathrm{as}+}_{m'}(i) \equiv \mathbf{v}^{\mathrm{as}+}_{m'}(\mathbf{r}-\boldsymbol{\varrho}_i)$. The elements (45) are diagonal in the azimuthal number m by cylindrical symmetry, they depend only on the vertical coordinate Z_i of the point $\mathbf{R}_i = \boldsymbol{\varrho}_i + Z_i\hat{\mathbf{e}}_z$, and they are real. Using these properties, the following asymptotic form of the wall Green's matrix (26) is obtained

$$G^{\mathrm{as}}_{ij}(lm\sigma|l'm'\sigma') = -\frac{6}{\pi\eta H^3}C(Z_i;lm\sigma)S_{\mathrm{cyl}}^{+-}(\boldsymbol{\varrho}_{ij};m|m')C(Z_j;l'm'\sigma'). \tag{46}$$

Due to the symmetric structure of the expression (46) and the symmetry property (37) of the scalar displacement matrix S_{cyl}^{+-}, the Lorentz symmetry

$$G^{\mathrm{as}}_{ij}(lm\sigma|l'm'\sigma') = G^{\mathrm{as}*}_{ji}(l'm'\sigma'|lm\sigma) \tag{47}$$

is manifest. We note that the presence of the Heaviside step function in relation (35) implies that

$$G^{\mathrm{as}}_{ij}(lm\sigma|l'm'\sigma') = 0 \quad \text{for } mm' \geqslant 0. \tag{48}$$

The physical interpretation of the matrix C follows from the expression

$$\mathbf{v}^{\mathrm{as}+}_{m}(\mathbf{r}-\boldsymbol{\varrho}_i) = \sum_{l\sigma} \mathbf{v}^{+}_{lm\sigma}(\mathbf{r}-\mathbf{R}_i)C(Z_i; lm\sigma), \tag{49}$$

which results from Eqs. (16) and (45). The matrix $C(Z; lm\sigma)$ thus describes the transformation from the representation of the flow in terms of nonsingular Hele–Shaw basis $\mathbf{v}^{\mathrm{as}+}_{m}(\mathbf{r}-\boldsymbol{\varrho}_i)$ centered at the lateral position $\boldsymbol{\varrho}_i$ to the spherical representation (12b) centered at $\mathbf{R}_i$.

4.5. Multipolar flow fields

An alternative interpretation of the matrix C is obtained by considering the far-field flow

$$\mathbf{u}^{\mathrm{as}}_{lm\sigma}(\mathbf{r}-\boldsymbol{\varrho}_2; Z_2) = \int \mathbf{T}^{\mathrm{as}}(\mathbf{r},\mathbf{r}')\delta^{\mathrm{S}}_{a}(\mathbf{r}'-\mathbf{R}_2)\mathbf{w}^{+}_{lm\sigma}(\mathbf{r}'-\mathbf{R}_2)\mathrm{d}\mathbf{r}' \tag{50}$$

produced in the space between the walls by the multipolar force density

$$\mathbf{F}(\mathbf{r}') = \delta^{\mathrm{S}}_{a}(\mathbf{r}'-\mathbf{R}_2)\mathbf{w}^{+}_{lm\sigma}(\mathbf{r}'-\mathbf{R}_2) \tag{51}$$

centered at $\mathbf{R}_2$. By inserting representation (43) specified for the shifted asymptotic Green's function (42) with $\boldsymbol{\varrho} = \boldsymbol{\varrho}_2$ into (50) and using definition (45) of the matrix C we find that

$$\mathbf{u}^{\mathrm{as}}_{lm\sigma}(\mathbf{r}-\boldsymbol{\varrho}_2; Z_2) = -\frac{6}{\pi\eta H^3}\mathbf{v}^{\mathrm{as}-}_{m}(\mathbf{r}-\boldsymbol{\varrho}_2)C(Z_2; lm\sigma). \tag{52}$$

Thus, the matrix element $C(Z_2; lm\sigma)$ represents the amplitude of the Hele–Shaw basis field $\mathbf{v}^{\mathrm{as}-}_{m}$ in the far-field multipolar velocity (50). Only one term contributes to this flow according to Eq. (52) because of the cylindrical symmetry of the problem.

The asymptotic multipolar flow fields (50) can also be expressed in terms of the matrix elements (46). To this end the right side of Eq. (50) is expanded in the spherical basis fields (12b) with the help of identity (16). The expansion yields the relation

$$\mathbf{u}^{\mathrm{as}}_{lm\sigma}(\mathbf{r}-\boldsymbol{\varrho}_2; Z_2) = \sum_{l'm'\sigma'} \mathbf{v}^{+}_{l'm'\sigma'}(\mathbf{r}-\mathbf{R}_1)G^{\mathrm{as}}_{12}(l'm'\sigma'|lm\sigma), \tag{53}$$

where G^{as}_{12} is given by Eq. (26) with the Green's function $\mathbf{T}$ replaced with $\mathbf{T}^{\mathrm{as}}$. The above expression relates the asymptotic flow $\mathbf{u}^{\mathrm{as}}_{lm\sigma}$ centered at the position $\mathbf{R}_2$ and the spherical basis fields centered at a different position $\mathbf{R}_1$.

We note that for each m only several force multipoles (51) produce a nonzero far-field velocity (50). This behavior results from the properties of the matrix $C(Z_2; lm\sigma)$ that appears in relation (52); the form of this matrix is analyzed in Section 4.6. A further discussion of the multipolar fields in the space between the walls is given in Appendix B.

4.6. Explicit expressions for the transformation matrix C

A general structure of the matrix C can be inferred using scaling arguments. According to Eq. (12b) spherical basis fields $\mathbf{v}^{+}_{lm\sigma}(\mathbf{r}-\mathbf{R}_i)$ are homogeneous functions of the order $l+\sigma-1$ of the relative-position vector $\mathbf{r}_i = \mathbf{r}-\mathbf{R}_i$. Similarly, Eqs. (31b) and (32) imply that the Hele–Shaw basis fields $\mathbf{v}^{\mathrm{as}+}_{m}(\mathbf{r}-\boldsymbol{\varrho}_i)$ are combinations of homogeneous functions of the order $|m|-1$, $|m|$, and $|m|+1$ of $\mathbf{r}_i$. Since the coefficients

$C(Z_i; lm\sigma)$ are independent of $\mathbf{r}_i$, relation (49) implies that the non-zero elements of $C(Z_i; lm\sigma)$ satisfy the condition

$$l + \sigma - |m| \leqslant 2. \tag{54}$$

A detailed analysis of relation (49) reveals that the nonzero elements of the matrix C can be written in the form [27]

$$C(Z; l \pm\mu\, \sigma) = B^{\pm}_{l-\mu\, \sigma}(Z; \mu), \quad \mu = |m| \geqslant 1, \tag{55}$$

where $B^{\pm}_{\lambda\sigma}(Z; \mu)$ are the elements of the 3×3 matrix

$$\left\{B^{\pm}_{\lambda\sigma}(Z; \mu)\right\}_{\lambda,\sigma=0,1,2} = \frac{1}{2}A^{\pm}(\mu)\begin{bmatrix} -Z(H-Z) & \mp(H-2Z) & 2 \\ \dfrac{-\mu(H-2Z)}{(\mu+1)(2\mu+3)^{1/2}} & \dfrac{\pm 2\mu}{(\mu+1)(2\mu+3)^{1/2}} & 0 \\ \dfrac{2\mu(\mu+1)^{1/2}}{(\mu+2)(2\mu+3)(\mu+5)^{1/2}} & 0 & 0 \end{bmatrix} \tag{56}$$

with

$$A^{\pm}(\mu) = (\mp 2)^{\mu}\mu!\left[\frac{4\pi}{(2\mu+1)(2\mu)!}\right]^{1/2}. \tag{57}$$

The range $\lambda = 0, 1, 2$ of the index $\lambda = l - |m|$ in Eq. (56) results from the conditions $|m| \leqslant l$ and (54). All other elements of the matrix C vanish.

We close our theoretical considerations with a remark that the asymptotic form G^{as}_{ij} of the Green's matrix G_{ij} is approached exponentially for $R_{ij} \to \infty$ because Liron–Mochon formula (39) is exponentially accurate at large distances. As in relation (39), the lengthscale for this approach is set by the wall separation H. The asymptotic expression (46) should thus be very accurate when the interparticle distance R_{ij} is larger than several wall separations H. This conclusion is supported by our numerical results discussed in the following section.

5. Numerical examples

5.1. Matrix elements

A typical behavior of the Green's matrix G_{ij} is illustrated in Figs. 1 and 2. The results are shown for the matrix elements

$$G_{12}(1\ -1\ 0|l\ \mu\ \sigma) = (-1)^{\sigma}G^{*}_{12}(110|l\ -\mu\ \sigma) \tag{58}$$

versus the lateral distance ϱ_{12} scaled by the wall separation H for several values of the parameters l, σ and $\mu > 0$. The elements (58) play a special role in our theory because in the asymptotic regime $\varrho_{12} \gg H$ they are directly related to the far-field multipolar flow (50) according to Eq. (B.7). In all examples, the vertical coordinates of the points (1) and (2) are $Z_1 = Z_2 = \frac{1}{4}H$. For other configurations the matrix elements have a similar behavior.

We present our results in the form of the rescaled elements defined by the relation

$$G_{12}(1\ \mp 1\ 0|l \pm\mu\ \sigma) = H^{\mu-l-\sigma+1}\tilde{G}_{12}(1\ \mp 1\ 0|l \pm\mu\ \sigma)\Phi^{-}_{\pm(\mu+1)}(\boldsymbol{\varrho}_{12}). \tag{59}$$

For those values of parameters l and μ for which the matrix elements (59) do not vanish, the factor $\Phi^{-}_{\pm(\mu+1)}(\boldsymbol{\varrho}_{12}) \sim \varrho_{12}^{-(\mu+1)}$ corresponds to the far-field behavior of $G^{\mathrm{as}}_{12}(1\ \mp 1\ 0|l \pm\mu\ \sigma)$, according to Eqs. (35)

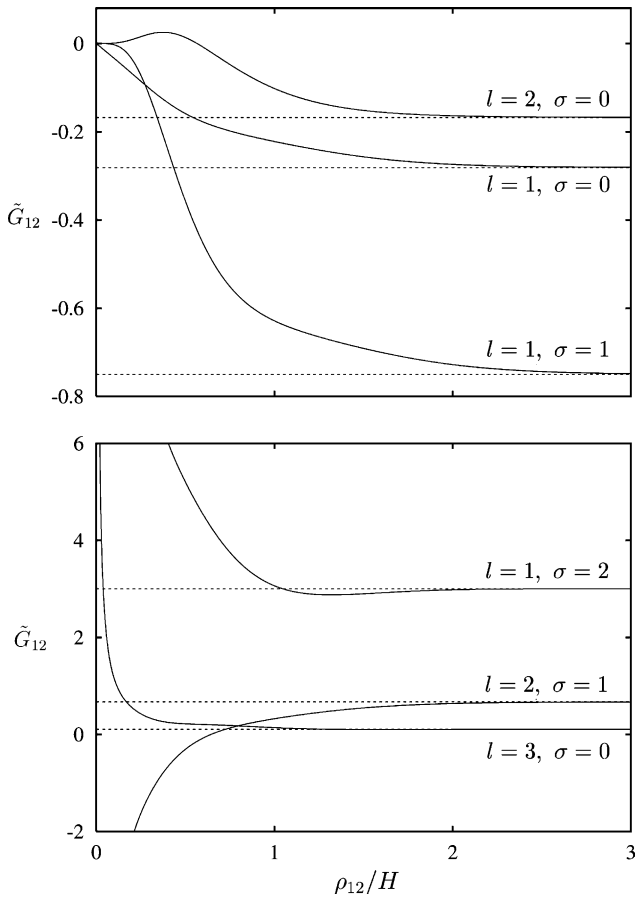

Fig. 1. Rescaled matrix elements $\tilde{G}_{12}(1\,-1\,0|l\,1\,\sigma)$ versus lateral distance ϱ_{12} for $Z_1 = Z_2 = \frac{1}{4}H$; values of parameters l and σ as labeled. Exact solution (solid lines); asymptotic behavior (dotted lines).

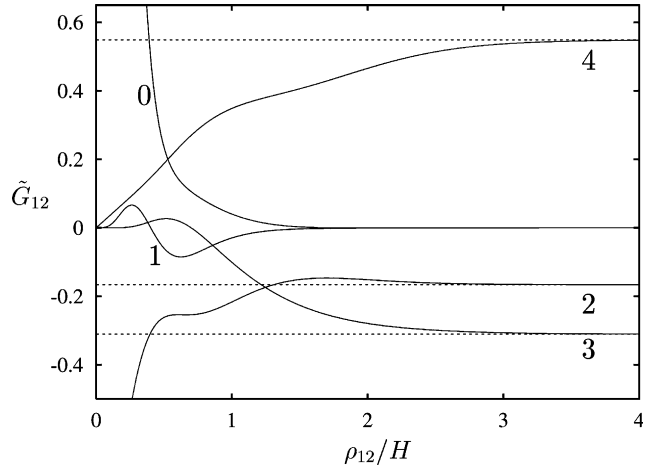

Fig. 2. Rescaled matrix elements $\tilde{G}_{12}(1\,-1\,0|4\,m\,0)$ versus lateral distance ϱ_{12} for $Z_1 = Z_2 = \frac{1}{4}H$; values of parameter m as labeled. Exact solution (solid lines); asymptotic behavior (dotted lines).

and (46). In the asymptotic regime $\varrho_{12} \gg H$ the rescaled elements $\tilde{G}^{\mathrm{as}}_{12}(1\ \mp 1\ 0|l\ \pm\mu\ \sigma)$ depend only on the vertical coordinates Z_1 and Z_2. The nonzero asymptotic elements are quadratic functions of the vertical coordinate Z_1, and they are at most quadratic in Z_2 but can also be linear or constant in this variable, as indicated by Eqs. (46) and (56). The far-field flow (50) is related to these elements by Eq. (B.9).

Fig. 1 illustrates the behavior of the matrix elements $\tilde{G}_{12}(1\ -1\ 0|l\ 1\ \sigma)$ with

$$l + \sigma \leqslant 3. \tag{60}$$

All these functions approach nonzero asymptotic values $\tilde{G}^{\mathrm{as}}_{12}(1\ -1\ 0|l\ 1\ \sigma) \neq 0$ for large interparticle distances $\varrho_{12} \gg H$, according to Eqs. (46) and (54). The corresponding behavior of the unscaled matrix elements (58)

$$G_{12}(1\ \mp 1\ 0|l\ \pm 1\ \sigma) \sim \varrho_{12}^{-2}, \quad \varrho_{12} \gg H, \tag{61}$$

follows from Eqs. (31a), (35), and (46).

The matrix elements (61) are directly related to the multipolar flow fields (50), as indicated by Eq. (B.7). Therefore, we find that Eq. (61) corresponds to the slowest possible far-field decay of the flow produced by a multipolar force distribution. The multipoles (60) include the horizontal Stokeslet ($l = 1$, $\sigma = 0$), rotlet ($l = 1$, $\sigma = 1$), stresslet ($l = 2$, $\sigma = 0$), and three other multipoles, one of which has the spherical-harmonics order $l = 3$. The numerical results shown in Fig. 1 indicate that the approach of $\tilde{G}_{12}$ to the asymptotic values is exponential, which is consistent with our discussion in Section 4.

Fig. 2 illustrates the behavior of matrix elements (58) for $l = 4$ and $\sigma = 0$. Unlike the elements presented in Fig. 1, the rescaled elements $\tilde{G}_{12}(1\ -1\ 0|4\ m\ 0)$ with $m = 0, 1$ vanish at large separations $\varrho \gg H$, which is consistent with condition (54). The remaining rescaled elements with $m = 2, 3, 4$ tend exponentially to nonzero asymptotic values.

5.2. Applications in multiparticle hydrodynamic-interactions algorithms

The simplest numerical application of our asymptotic formulas (46), (55), and (56) is to implement them directly in the induced-force-multipole equation (21). To this end, the matrix (26) is represented as the superposition of the long-range asymptotic part and the short-range correction, i.e.

$$G_{ij}(lm\sigma|l'm'\sigma') = G^{\mathrm{as}}_{ij}(lm\sigma|l'm'\sigma') + \delta G_{ij}(lm\sigma|l'm'\sigma'). \tag{62}$$

The asymptotic part $G^{\mathrm{as}}_{ij}(lm\sigma|l'm'\sigma')$ can be evaluated from our explicit formulas at a low numerical cost. To obtain the correction term $\delta G_{ij}(lm\sigma|lm\sigma)$, first the expression $G_{ij}(lm\sigma|l'm'\sigma')$ is calculated using the Cartesian-representation method described in [14,15] and next, the asymptotic expression is subtracted from the result. Since the correction term is short ranged, the matrix $\delta G_{ij}(lm\sigma|l'm'\ \sigma')$ can be truncated by setting

$$\delta G_{ij}(lm\sigma|l'm'\sigma') = 0 \quad \text{for } \varrho_{ij} > \varrho_{\mathrm{as}}, \tag{63}$$

where the truncation distance ϱ_{as} is of the order of several wall separations H. The results shown in Figs. 1 and 2 and other similar tests indicate that the asymptotic approximation for the Green's matrix is very accurate for $\varrho_{\mathrm{as}} \gtrsim 3H$. Thus, the numerically expensive contribution δG_{ij} has to be evaluated only for the neighboring particles at an O(N) cost.

To test our asymptotic approach and illustrate the role of the long- and short-range contributions to the Green's matrix G, we consider a benchmark case of a linear rigid array of N touching spheres translating in the center plane in the space between closely spaced walls. The spheres are on a line parallel to the x direction and the array is moving either in the x (longitudinal) or y (transverse) direction. We focus on the translational friction coefficients evaluated per particle

$$\bar{\zeta}^{\alpha\alpha}_{\mathrm{C}} = (N\zeta_{\parallel})^{-1} \sum_{i,j=1}^{N} \zeta^{\mathrm{tt}\alpha\alpha}_{ij}, \quad \alpha = x, y, \tag{64}$$

where $\zeta_{ij}^{\mathrm{tt}\alpha\alpha}$ is the $\alpha\alpha$ component of the translational resistance tensor $\boldsymbol{\zeta}_{ij}^{\mathrm{tt}}$ defined in Eq. (2), and $\zeta_{\parallel}$ is the one-particle lateral translational resistance coefficient [16,14].

As illustrated in Fig. 3 (see also discussion in [15,14]) the longitudinal and transverse friction coefficients (64) behave differently. The longitudinal coefficient $\bar{\zeta}_{\mathrm{C}}^{xx}$ decreases with the length of the array N, while the transverse coefficient $\bar{\zeta}_{\mathrm{C}}^{yy}$ increases with N. For tight configurations with small gaps between the wall and particle surfaces (the case show in Fig. 3) the decrease of $\bar{\zeta}_{\mathrm{C}}^{xx}$ is moderate because the friction force is dominated by the local resistance due to the dissipation in these gaps. In contrast, the increase of $\bar{\zeta}_{\mathrm{C}}^{yy}$ is large due to collective long-range effects.

The mechanism of these collective effects can be explained using the results for the pressure field around arrays of the length $N = 10$ and 20 plotted in Figs. 4 and 5. The figures show the normalized asymptotic far-field pressure

$$\bar{p}^{\mathrm{as}} = H(\eta U)^{-1} p^{\mathrm{as}} \tag{65}$$

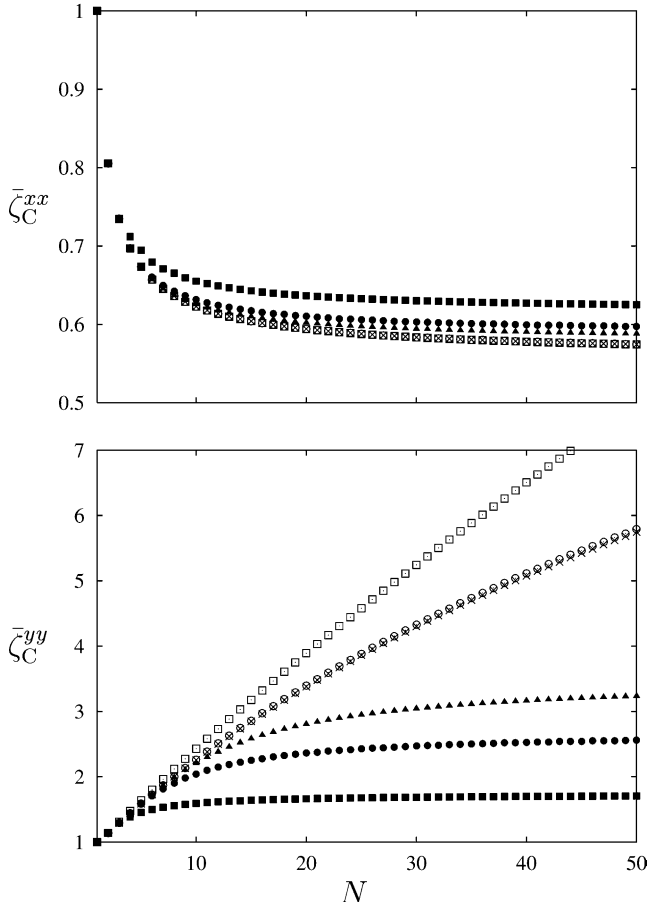

Fig. 3. Normalized longitudinal and transverse friction coefficients per particle $\bar{\zeta}_{\mathrm{C}}^{xx}$ and $\bar{\zeta}_{\mathrm{C}}^{yy}$ for linear arrays of touching spheres in the center plane between the walls, for wall separation $H/2a = 1.05$. Crosses represent exact results; open symbols represent asymptotic approximation (63) with $\varrho_{\mathrm{as}}/H = 1$ (squares) and 2 (circles); solid symbols correspond to truncation (66) with $\varrho_0/H = 2$ (squares), 4 (circles) and 6 (triangles). For the longitudinal coefficient $\bar{\zeta}_{\mathrm{C}}^{xx}$ the open squares and circles coincide with the crosses.

(where U is the velocity of the array), which was evaluated using the method described in Appendix C. The results for the longitudinal motion of the array shown in Figs. 4(a) and 5(a) indicate that the pressure field is only weakly affected by the length of the array, and its magnitude is the largest near the array ends. In contrast, the pressure shown in Figs. 4(b) and 5(b) for the transverse motion increases approximately linearly with the array length N, and its magnitude is maximal near the chain center. This large pressure amplitude is associated with the flow of the displaced fluid around the ends of the array in the confined space. The flow is significant over the distance that scales with the length of the array $l = 2Na$ (where a is the sphere radius). In the Hele–Shaw regime the pressure gradient is proportional to the fluid velocity; hence, the pressure itself is proportional to N.

To further elucidate the effects of the short-range and far-field flow components, the exact numerical results for the resistance coefficients (64) are compared in Fig. 3 with the asymptotic approximation (62) and (63). We also show results obtained using a much cruder approximation, where the *whole* Green's matrix is truncated at a certain distance ϱ_0, i.e.

$$G_{ij}(lm\sigma|l'm'\sigma') = 0 \quad \text{for } \varrho_{ij} > \varrho_0. \tag{66}$$

Our numerical calculations indicate that the truncation (66) yields poor results. The far-field flow contribution is especially important for the transverse motion of the array because of the positive-feedback effect: For this motion the dipolar Hele–Shaw flow field generated by a given particle acts as a back flow on the other particles. This back flow, in turn, produces an increase in the induced force distribution that generates the dipolar flow. This back flow mechanism, resulting in the large transverse resistance, is consistent with our discussion of the pressure field shown in Figs. 4(b) and 5(b).

In contrast to the crude approximation (66), a truncation of the short-range part (63) of the Green's matrix yields accurate results already with moderate values of the truncation parameter ϱ_{as}. The results shown in Fig. 3 indicate that the truncations at $\varrho_{as}/H = 1$ for the longitudinal motion and at $\varrho_{as}/H = 2$ for the transverse motion are sufficient. The results with $\varrho_{as}/H \geqslant 3$ (not shown) are essentially indistinguishable from the exact results.

Application of our far-field asymptotic expressions in the algorithm for evaluation of many-particle hydrodynamic friction and mobility matrices yields a substantial reduction of the numerical cost. As an example we consider the calculation times for the friction coefficients (64) in the configuration corresponding to the results in Fig. 3. To obtain these coefficients with accuracy better than 2%, the Green's matrix $G_{ij}(lm\sigma|l'm'\sigma')$ has to be determined for $l, l' \leqslant l_{max}$, where $l_{max} = 4$. The highly accurate results shown in Fig. 3 have been obtained using $l_{max} = 6$.

On a standard 2.5 GHz work station, evaluation of the matrix G_{ij} with $l_{max} = 4$, using truncation (63) of the short-range contributions at $\varrho_{as}/H = 2$, requires 2 s for $N = 10$ particles, 6 s for $N = 20$, and 14 s for $N = 40$. As expected, the evaluation time grows approximately linearly with N because it is dominated by the $O(N)$ calculation of the exact matrix elements for the neighboring particles. When all $O(N^2)$ matrix elements are determined from the exact Fourier-integral formulas [14,15], the corresponding calculation times are 9, 70, and 560 s, respectively. The calculation time grows faster than $O(N^2)$ with the system size, because for widely separated particles in long chains, evaluation of the Fourier integrals requires a large number of integration points due to the oscillatory character of the integrands.

The numerical tests, described above, indicate that the implementation of the asymptotic expressions in our hydrodynamic-interaction algorithm may reduce numerical cost by almost two orders of magnitude even for a relatively small system of $N = 40$ particles. We also note that the simplification afforded by our asymptotic analysis will facilitate constructing $O(N)$ accelerated algorithms. Furthermore, our asymptotic formulas can be used to develop efficient simulation techniques for doubly periodic wall-bounded suspensions. These applications are discussed at the end of the following section.

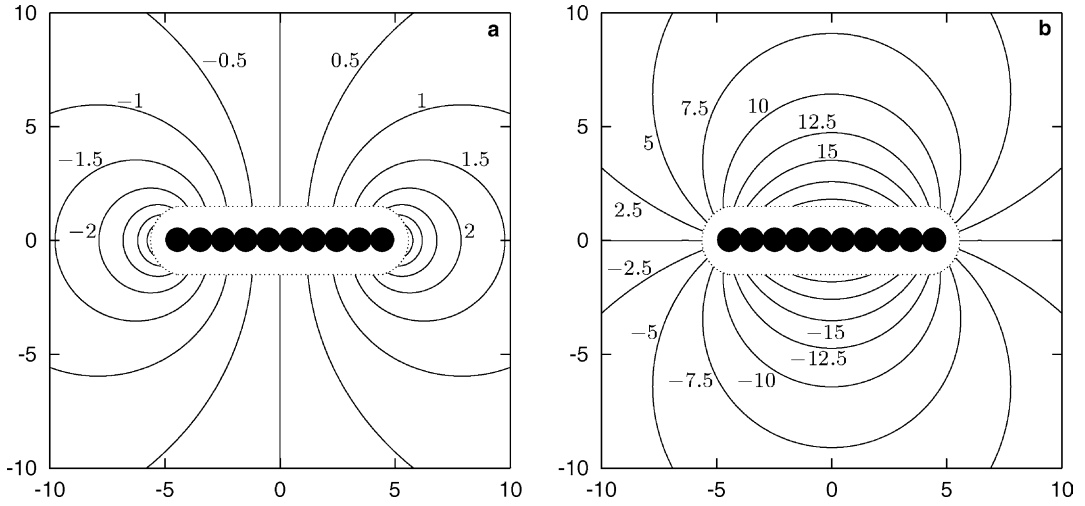

Fig. 4. Contour plots of the normalized asymptotic pressure field (65) around a rigid array of $N = 10$ touching spheres moving in the center plane between parallel walls, for wall separation $H/2a = 1.05$. Longitudinal motion (a); transverse motion (b). The dotted lines delimit the regions where the asymptotic approximation is not valid.

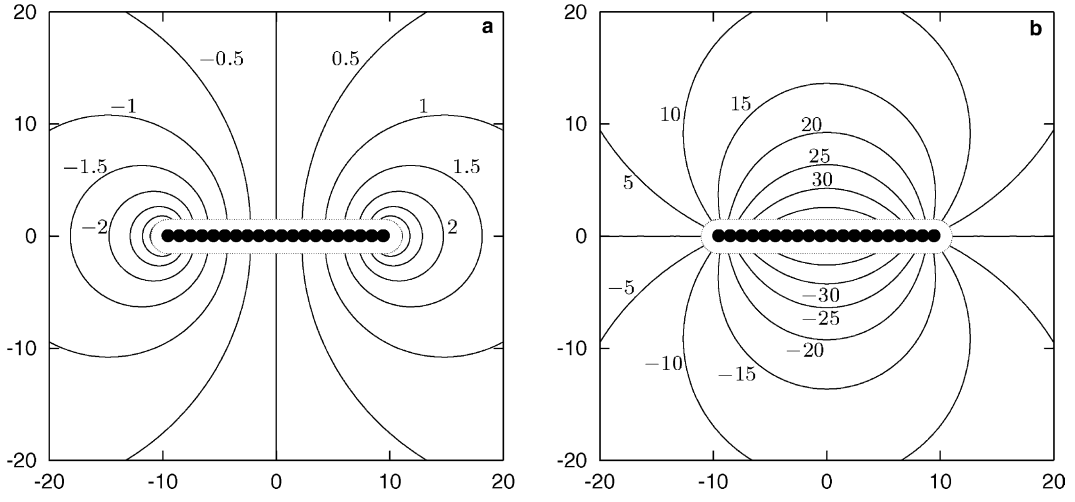

Fig. 5. Same as Fig. 4, except that for $N = 20$.

6. Conclusions

Our paper presents a complete analysis of the far-field flow produced by an arbitrary force multipole in the space bounded by two parallel planar walls. We have shown that a force multipole characterized by the multipolar numbers $lm\sigma$ produces, at large distances, a Hele–Shaw flow driven by a two-dimensional multipolar pressure field of the azimuthal order m. The amplitude of this flow has been explicitly obtained for an arbitrary order of the source force multipole.

Our asymptotic results were applied to evaluate the multipolar matrix elements $G_{ij}(lm\sigma|l'm'\sigma')$ of the Green's tensor for Stokes flow in the wall-bounded domain. This matrix is used in our recently developed algorithm [14,15] for evaluation of the multiparticle friction tensor ζ_{ij} in a suspension confined between two

parallel walls. The elements of the matrix G_{ij} are equivalent to the expansion coefficients in the displacement theorem for Stokes flow in the bounded domain. Such a displacement theorem relates the flow produced by a force multipole centered at a point $\mathbf{R}_j$ to nonsingular multipolar flows centered at a point $\mathbf{R}_i$. We have shown that in the far-field regime the matrix elements $G_{ij}(lm\sigma|l'm'\sigma')$ can be expressed in terms of much simpler displacement formulas for the two-dimensional scalar potential.

We have found that the matrix G_{ij} achieves its asymptotic behavior when the lateral distance between the centers of the particles i and j exceeds several wall separations H. Evaluation of the exact matrix elements in terms of lateral Fourier integrals derived in [15,14] is thus needed only for the neighboring particles. Therefore, application of the asymptotic expressions in our hydrodynamic-interaction algorithm yields an important improvement of its numerical efficiency. (The far-field contribution to the Green's matrix cannot be simply neglected—for some problems such a crude approximation leads to entirely wrong values of the friction matrix; cf. discussion in Section 5.2).

Several other important consequences stem from the fact that we have reduced a complex hydrodynamic problem to a simpler problem of a two-dimensional scalar potential. First, since for a scalar potential the multipolar flow fields in a periodic system are known [30], the results of our analysis can be used to develop an algorithm for hydrodynamic interactions in a periodic wall-bounded system. Without the asymptotic expressions, evaluation of the periodic hydrodynamic Green's matrix would be much more difficult, as discussed in [27].

Next, for scalar potentials, fast multipole and PPPM acceleration techniques are well developed [31]. Combined with our asymptotic results, such methods can be applied for fast evaluation of hydrodynamic interactions in wall-bounded suspensions. Development of accelerated algorithms for suspensions will require implementation of certain techniques that are specific to multiparticle hydrodynamic systems, e.g. an appropriate preconditioning of the Green's matrix and incorporating the lubrication interactions into the calculation scheme. These techniques were used in accelerated Stokesian-dynamics algorithms for unbounded suspensions [32, 33]. Our present asymptotic results greatly facilitate development of accelerated algorithms for wall-bounded systems, and our research is currently focused on this problem.

Acknowledgments

S.B. would like to acknowledge the support by NSF Grant CTS-0201131. E.W. was supported by NASA Grant NAG3-2704 and, in part, by KBN Grant No. 5T07A 052 24. J.B. was supported by NSF Grant CTS-0348175.

Appendix A. Spherical basis

The spherical basis sets of Stokes flows $\mathbf{v}^{\pm}_{lm\sigma}$ used in the present paper are normalized differently than the corresponding sets $\mathbf{v}^{\pm(\mathrm{CFS})}_{lm\sigma}$ introduced in [21]. The transformations between the basis fields are

$$\mathbf{v}^{-}_{lm\sigma}(\mathbf{r}) = N^{-1}_{l\sigma} n^{-1}_{lm} \mathbf{v}^{-(\mathrm{CFS})}_{lm\sigma}(\mathbf{r}), \tag{A.1a}$$

$$\mathbf{v}^{+}_{lm\sigma}(\mathbf{r}) = N_{l\sigma} n^{-1}_{lm} \mathbf{v}^{+(\mathrm{CFS})}_{lm\sigma}(\mathbf{r}), \tag{A.1b}$$

where

$$N_{l0} = 1, \tag{A.2a}$$

$$N_{l1} = -(l+1)^{-1}, \tag{A.2b}$$

$$N_{l2} = l[(l+1)(2l+1)(2l+3)]^{-1} \tag{A.2c}$$

and

$$n_{lm} = \left[\frac{4\pi}{2l+1}\frac{(l+m)!}{(l-m)!}\right]^{1/2}. \tag{A.3}$$

Below we list the explicit expressions for the angular coefficients $\mathbf{V}^{\pm}_{lm\sigma}(\theta,\phi)$ for spherical basis fields (12) in our present normalization

$$\mathbf{V}^{-}_{lm0} = \frac{1}{(2l+1)^2}\left[\frac{l+1}{l(2l-1)}\alpha_l \mathbf{Y}_{ll-1m} - \frac{1}{2}\mathbf{Y}_{ll+1m}\right], \tag{A.4a}$$

$$\mathbf{V}^{-}_{lm1} = \frac{\mathrm{i}}{l+1}\gamma_l \mathbf{Y}_{llm}, \tag{A.4b}$$

$$\mathbf{V}^{-}_{lm2} = \beta_l \mathbf{Y}_{ll+1m} \tag{A.4c}$$

and

$$\mathbf{V}^{+}_{lm0} = \alpha_l \mathbf{Y}_{ll-1m}, \tag{A.5a}$$

$$\mathbf{V}^{+}_{lm1} = \frac{\mathrm{i}}{l+1}\gamma_l \mathbf{Y}_{llm}, \tag{A.5b}$$

$$\mathbf{V}^{+}_{lm2} = \frac{l}{2(2l+1)}\alpha_l \mathbf{Y}_{ll-1m} + \frac{l}{(l+1)(2l+1)(2l+3)}\beta_l \mathbf{Y}_{ll+1m}, \tag{A.5c}$$

where

$$\mathbf{Y}_{ll-1m}(\hat{\mathbf{r}}) = \alpha_l^{-1} r^{-l+1}\nabla\left[r^l Y_{lm}(\hat{\mathbf{r}})\right], \tag{A.6a}$$

$$\mathbf{Y}_{ll+1m}(\hat{\mathbf{r}}) = \beta_l^{-1} r^{l+2}\nabla\left[r^{-(l+1)} Y_{lm}(\hat{\mathbf{r}})\right], \tag{A.6b}$$

$$\mathbf{Y}_{llm}(\hat{\mathbf{r}}) = \gamma_l^{-1}\mathbf{r}\times\nabla_{\mathrm{s}} Y_{lm}(\hat{\mathbf{r}}) \tag{A.6c}$$

are the normalized vector spherical harmonics, as defined by [34]. Here

$$Y_{lm}(\hat{\mathbf{r}}) = n_{lm}^{-1}(-1)^m P_l^m(\cos\theta)e^{\mathrm{i}m\varphi} \tag{A.7}$$

are the normalized scalar spherical harmonics, and

$$\alpha_l = [l(2l+1)]^{1/2}, \tag{A.8a}$$

$$\beta_l = [(l+1)(2l+1)]^{1/2}, \tag{A.8b}$$

$$\gamma_l = -\mathrm{i}[l(l+1)]^{1/2}. \tag{A.8c}$$

Appendix B. Flow fields generated by force multipoles

In this Appendix B, we express the flow field

$$\mathbf{u}_{lm\sigma}(\mathbf{r}-\boldsymbol{\varrho}_2;Z_2) = \int \mathbf{T}(\mathbf{r},\mathbf{r}')\delta_a^{\mathrm{S}}(\mathbf{r}'-\mathbf{R}_2)\mathbf{w}^{+}_{lm\sigma}(\mathbf{r}'-\mathbf{R}_2)\mathrm{d}\mathbf{r}' \tag{B.1}$$

produced in the space between the walls by the force multipole (51) in terms of the elements of the Green's matrix G_{12}. Using relation (16) to expand the right-hand side of Eq. (B.1) into the non-singular spherical basis fields (12b) yields

$$\mathbf{u}_{lm\sigma}(\mathbf{r}-\boldsymbol{\varrho}_2;Z_2) = \sum_{l'm'\sigma'}\mathbf{v}^{+}_{l'm'\sigma'}(\mathbf{r}-\mathbf{R}_1)G_{12}(l'm'\sigma'|lm\sigma), \tag{B.2}$$

where the definition (26) of the Green's matrix have been used. Eq. (53) is the asymptotic form of the above relation.

Eq. (B.2) can be simplified by evaluating it for $\mathbf{r} = \mathbf{R}_1$ and noting that

$$\mathbf{v}^{+}_{l'm'\sigma'}(0) = 0 \quad \text{for } l' + \sigma' > 1 \tag{B.3}$$

and

$$\mathbf{v}^{+}_{1m'0}(0) = \left(\frac{4}{3}\pi\right)^{-1/2} \hat{\mathbf{e}}_{m'}, \tag{B.4}$$

where $m' = 0, \pm 1$, and

$$\hat{\mathbf{e}}_{\pm 1} = \mp \frac{1}{\sqrt{2}}(\hat{\mathbf{e}}_x \pm \mathrm{i}\hat{\mathbf{e}}_y), \quad \hat{\mathbf{e}}_0 = \hat{\mathbf{e}}_z, \tag{B.5}$$

which follows from Eq. (A.5a). According to the above expressions, only three terms of the sum (B.2) contribute to the result,

$$\mathbf{u}_{lm\sigma}(\mathbf{R}_1 - \boldsymbol{\varrho}_2; Z_2) = \left(\frac{4}{3}\pi\right)^{-1/2} \sum_{m'=-1,0,1} G_{12}(1m'0|lm\sigma)\hat{\mathbf{e}}_{m'}. \tag{B.6}$$

In the asymptotic regime $\varrho_{12} \gg H$ this relation simplifies because the asymptotic matrix elements (46) vanish for $m'm \geqslant 0$, as discussed in Section 4. Taking this observation into account we thus find

$$\mathbf{u}^{\mathrm{as}}_{l\ \pm\mu\ \sigma}(\mathbf{R}_1 - \boldsymbol{\varrho}_2; Z_2) = \left(\frac{4}{3}\pi\right)^{-1/2} G^{\mathrm{as}}_{12}(1\ \mp 1\ 0|l\ \pm\mu\ \sigma)\hat{\mathbf{e}}_{\mp 1}, \tag{B.7}$$

where $\mu = 1, 2, \ldots$ The dependence of the flow field (B.7) on the lateral relative-position vector $\boldsymbol{\varrho}_{12}$ can be made more explicit by using relation (59) and the identity

$$\Phi_{\pm(\mu+1)}(\boldsymbol{\varrho}_{12})\hat{\mathbf{e}}_{\mp 1} = \mp 2^{-1/2}(\mu+1)^{-1}\boldsymbol{\nabla}_{\parallel}\Phi^{-}_{\pm\mu}(\boldsymbol{\varrho}_{12}), \tag{B.8}$$

which yields

$$\mathbf{u}^{\mathrm{as}}_{l\ \pm\mu\sigma}(\mathbf{R}_1 - \boldsymbol{\varrho}_2; Z_2) = \mp\left(\frac{8}{3}\pi\right)^{-1/2}(\mu+1)^{-1}H^{\mu-l-\sigma+1}\tilde{G}^{\mathrm{as}}_{12}(1\ \mp 1\ 0|l\ \pm\mu\ \sigma)\boldsymbol{\nabla}_{\parallel}\Phi^{-}_{\pm\mu}(\boldsymbol{\varrho}_{12}). \tag{B.9}$$

We note that relation (B.9) is consistent with (52) due to Eq. (32).

Appendix C. Far-field pressure distribution

As discussed in Section 4, the flow and the pressure fields in the Hele–Shaw asymptotic regime (27) are uniquely related (up to an additive constant in the pressure). Thus, many of the asymptotic formulas, expressed here in terms of the velocity fields, can be translated into the corresponding expressions for the pressure.

This remark applies, in particular, to Eq. (52) for the asymptotic multipolar flow (50). We introduce the asymptotic multipolar pressure field $p^{\mathrm{as}}_{lm\sigma}(\mathbf{r})$, which is defined by the relation

$$\mathbf{u}^{\mathrm{as}}_{lm\sigma}(\mathbf{r} - \boldsymbol{\varrho}_2; Z_2) = -\frac{1}{2}\eta^{-1}z(H-z)\nabla_{\parallel}p^{\mathrm{as}}_{lm\sigma}(\boldsymbol{\rho} - \boldsymbol{\varrho}_2; Z_2). \tag{C.1}$$

Using Eqs. (30) and (32), the flow-field identity (52) can be transformed into the corresponding pressure identity of the form

$$p^{\mathrm{as}}_{lm\sigma}(\boldsymbol{\rho}-\boldsymbol{\varrho}_2;Z_2) = -\frac{6}{\pi H^3}\Phi^-_m(\boldsymbol{\rho}-\boldsymbol{\varrho}_2)C(Z_2;lm\sigma). \tag{C.2}$$

Eq. (C.2) can be conveniently used to evaluate the far-field disturbance pressure p^{as} in a many-particle system. This equation describes the asymptotic pressure produced in the far-field regime by a single force multipole (51), as indicated by Eqs. (50) and (C.1). To determine p^{as}, the multipolar moments $f_i(lm\sigma)$ of the force distributions (18) induced on the surfaces of particles $i = 1,\ldots,N$ are evaluated by solving the force-multipole Eq. (21). Combining the solution with (C.2) yields

$$p^{\mathrm{as}}(\boldsymbol{\rho}) = \sum_{i=1}^{N}{\sum_{m}}' Q_i(m)\Phi^-_m(\boldsymbol{\rho}-\boldsymbol{\varrho}_i), \tag{C.3}$$

where

$$Q_i(m) = -\frac{6}{\pi H^3}\sum_{l\sigma} C(Z_i;lm\sigma)f_i(lm\sigma). \tag{C.4}$$

The contour plots in Figs. 4 and 5 were obtained using this method.

References

[1] H. Acuña Campa, M.D. Carbajal-Tinoco, J.L. Arauz-Lara, M. Medina-Noyola, Collective dynamics in quasibidimensional colloidal suspensions, Phys. Rev. Lett. 80 (1998) 5802–5805.

[2] R. Pesché, M. Kollmann, G. Nägele, Brownian dynamics study of dynamic scaling and related freezing criteria in quasi-two-dimensional dispersions, J. Chem. Phys. 114 (2001) 8701–8707.

[3] J. Santana-Solano, J.L. Arauz-Lara, Short-time dynamics of colloidal particles confined between two walls, Phys. Rev. E 65 (2002) 021406-1–021406-8.

[4] E.J. Stancik, A.L. Hawkinson, Dynamic transitions and oscillatory melting of a two-dimensional crystal subjected to shear flow, J. Rheol. 48 (2003) 159–173.

[5] I. Cohen, T.G. Mason, D.A. Weitz, Shear-induced configurations of confined colloidal suspensions, Phys. Rev. Lett. 93 (2004) 046001.

[6] Y.L. Chen, M.D. Graham, J.J. de Pablo, G.C. Randall, M. Gupta, P.S. Doyle, Conformation and dynamics of single DNA molecules in parallel-plate slit microchannels, Phys. Rev. E 70 (2004) 060901(R).

[7] L.J. Durlofsky, J.F. Brady, Dynamic simulation of bounded suspensions of hydrodynamically interacting particles, J. Fluid. Mech. 200 (1989) 39–67.

[8] M.E. Staben, A.Z. Zinchenko, R.H. Davis, Motion of a particle between two parallel plane walls in low-Reynolds-number Poiseuille flow, Phys. Fluids. 15 (2003) 1711–1733.

[9] N. Liron, S. Mochon, Stokes flow for a stokeslet between two parallel flat plates, J. Engineering Math. 10 (1976) 287–303.

[10] S. Bhattacharya, J. Bławzdziewicz, Image system for Stokes-flow singularity between two parallel planar walls, J. Math. Phys. 43 (2002) 5720–5731.

[11] P. Nott, J. Brady, Pressure-driven flow of suspensions—simulation and theory, J. Fluid Mech. 275 (1994) 157–199.

[12] L. Lobry, N. Ostrowsky, Diffusion of Brownian particles trapped between two walls: Theory and dynamic-light-scattering measurements, Phys. Rev. B 53 (1996) 12050–12056.

[13] R. Pesché, G. Nägele, Stokesian dynamics study of quasi-two-dimensional suspensions confined between two parallel walls, Phys. Rev. E 62 (2000) 5432–5443.

[14] S. Bhattacharya, J. Bławzdziewicz, E. Wajnryb, Hydrodynamic interactions of spherical particles in suspensions confined between two planar walls, J. Fluid Mech. in press.

[15] S. Bhattacharya, J. Bławzdziewicz, E. Wajnryb, Many-particle hydrodynamic interactions in parallel-wall geometry: Cartesian-representation method, Physica A 356 (2005) 294.

[16] R.B. Jones, Spherical particle in Poiseuille flow between planar walls, J. Chem. Phys. 121 (2004) 483–500.

[17] R.G. Cox, H. Brenner, Effect of finite boundaries on Stokes resistance of an arbitrary particle. 3. Translation and rotation, J. Fluid Mech. 28 (1967) 391.

[18] P. Mazur, D. Bedeaux, A generalization of Faxén's theorem to nonsteady motion of a sphere through an incompressible fluid in arbitrary flow, Physica 76 (1974) 235–246.

[19] B.U. Felderhof, Force density induced on a sphere in linear hydrodynamics. II. Moving sphere, mixed boundary conditions, Physica A 84 (1976) 569–576.
[20] R.B. Jones, R. Schmitz, Mobility matrix for arbitrary spherical particles in solution, Physica A 149 (1988) 373–394.
[21] B. Cichocki, B.U. Felderhof, R. Schmitz, Hydrodynamic interactions between two spherical particles, PhysicoChem. Hyd. 10 (1988) 383–403.
[22] J. Bławzdziewicz, E. Wajnryb, M. Loewenberg, Hydrodynamic interactions and collision efficiencies of spherical drops covered with an incompressible surfactant film, J. Fluid Mech. 395 (1999) 29–59.
[23] B. Cichocki, B.U. Felderhof, K. Hinsen, E. Wajnryb, J. Bławzdziewicz, Friction and mobility of many spheres in Stokes flow, J. Chem. Phys. 100 (1994) 3780–3790.
[24] B. Cichocki, R.B. Jones, R. Kutteh, E. Wajnryb, Friction and mobility for colloidal spheres in Stokes flow near a boundary: The multipole method and applications, J. Chem. Phys. 112 (2000) 2548–2561.
[25] G.S. Perkins, R.B. Jones, Hydrodynamic interaction of a spherical particle with a planar boundary. 1. Free-surface, Physica A 171 (1991) 575–604.
[26] B.U. Felderhof, R.B. Jones, Displacement theorems for spherical solutions of the linear Navier–Stokes equations, J. Math. Phys. 30 (1989) 339–342.
[27] S. Bhattacharya, Hydrodynamic interactions in confined geometries, Ph.D. thesis, Yale University (2005).
[28] C.M. Bender, S.A. Orszag, Advanced Mathematical Methods for Scientists and Engineers: Asymptotic Methods and Perturbation Theory, Springer-Verlag, New York, 1999.
[29] W.W. Hackborn, Asymmetric Stokes flow between parallel planes due to a rotlet, J. Fluid Mech. 218 (1990) 531–546.
[30] B. Cichocki, B.U. Felderhof, Electrostatic interactions in two-dimensional Coulomb systems with periodic boundary conditions, Physica A 158 (1989) 706–722.
[31] D. Frenkel, B. Smit, Understanding Molecular Simulation. From Algorithms to Simulations, Academic Press, New York, 2002.
[32] A. Sierou, J.F. Brady, Accelerated Stokesian dynamics simulations, J. Fluid Mech. 448 (2001) 115–146.
[33] A.S. Sangani, G.B. Mo, An O(N) algorithm for Stokes and Laplace interactions of particles, Phys. Fluids 8 (1996) 1990–2010.
[34] A.R. Edmonds, Angular Momentum in Quantum Mechanics, Princeton University Press, Princeton, 1960.